CHAPTER 4

MICROSTRUCTURAL CHARACTERIZATION AND MECHANICAL PROPERTIES OF A356-Mg_2Si-TiB_2 HYBRID COMPOSITES

4.1 INTRODUCTION

The chapter provides chemical compositions of base A356 alloy and hybrid composites. The results and interpretations of XRD analysis of base alloy and composites for phase identification are also presented. The optical and scanning electron microscopes were employed to analyse the microstructural characteristics of composites produced by the stir casting and cooling slope (CS) casting techniques. The influence of CS casting on the microstructure and particle size, morphology, and phase distributions in the matrix have been discussed in details.

4.2 CHEMICAL COMPOSITION of A356 ALLOY

Table 4.1 presents the chemical composition of the matrix measured using Optical Emission Spectrometer (Foundry Master). The reported results are average of three samples taken at different locations.

Table 4.1 Elemental composition of A356 alloy

Elements	Si	Mg	Cu	Fe	Mn	Zn	Ni	Al
Weight %	7.10	0.25	0.11	0.20	0.03	0.05	0.06	Bal.

4.3 X-RAY DIFFRACTION (XRD) ANALYSIS

Figure 4.1 displays the XRD pattern of matrix A356 alloy and composites with 10% Mg_2Si and varying amounts of TiB_2 phase 0, 1, 3, and 5wt.%.

It indicates that the mono- composite consist only the peaks of Mg_2Si; however, the hybrid composites comprise the peaks of Mg_2Si and TiB_2. It indicates that the Mg_2Si and TiB_2 phases are successfully formed in the hybrid composites by the insitu reactions. The TiB_2 phase is produced by the aluminothermic reaction between inorganic salts K_2TiF_6 and KBF_4 and molten aluminium. No other possible phases like Al_3Ti and AlB_2 are observed in XRD patterns that also indicate completion of reaction.

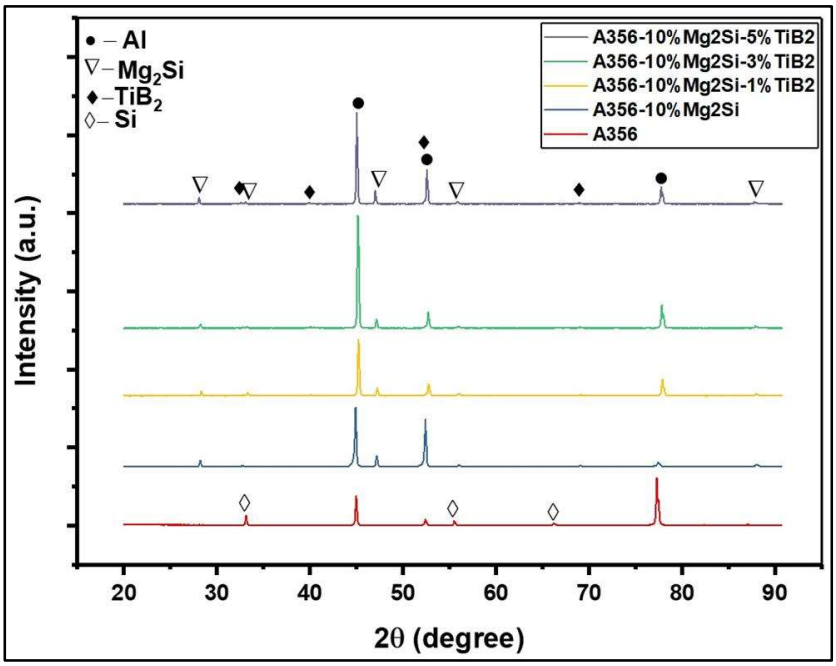

Fig. 4.1 XRD patterns of base alloy (A356) and A356-10Mg_2Si-xTiB_2 composites (x= 0, 1, 3 and 5)

4.4 MICROSTRUCTURAL AND MECHANICAL CHARACTERISTICS OF HYBRID COMPOSITES IN STIR CAST CONDITIONS

4.4.1 Density and Porosity measurement

Figure 4.2 (a) and (b) show the theoretical density, actual density and porosity percentage of base alloy and composites having various amount of TiB_2 particles. Fig. 2 (a) indicates that adding Mg in the alloy, density of the composite decreases owing to lower density of Mg_2Si phase (1.99 g/cm^3). However, porosity in the composite increases compared with the alloy as displayed in Fig. 4.2 (b). It can be attributed to the less freezing range of the alloy than the composites. Density of hybrid composite slightly

increases as the TiB_2 particles content increases due to higher density of TiB_2 (4.52 g/cm^3) than the matrix alloy. Porosity in hybrid composite increases with increase of TiB_2 particles owing to agglomeration of TiB_2 particles and difference in coefficient of thermal expansion. [39].

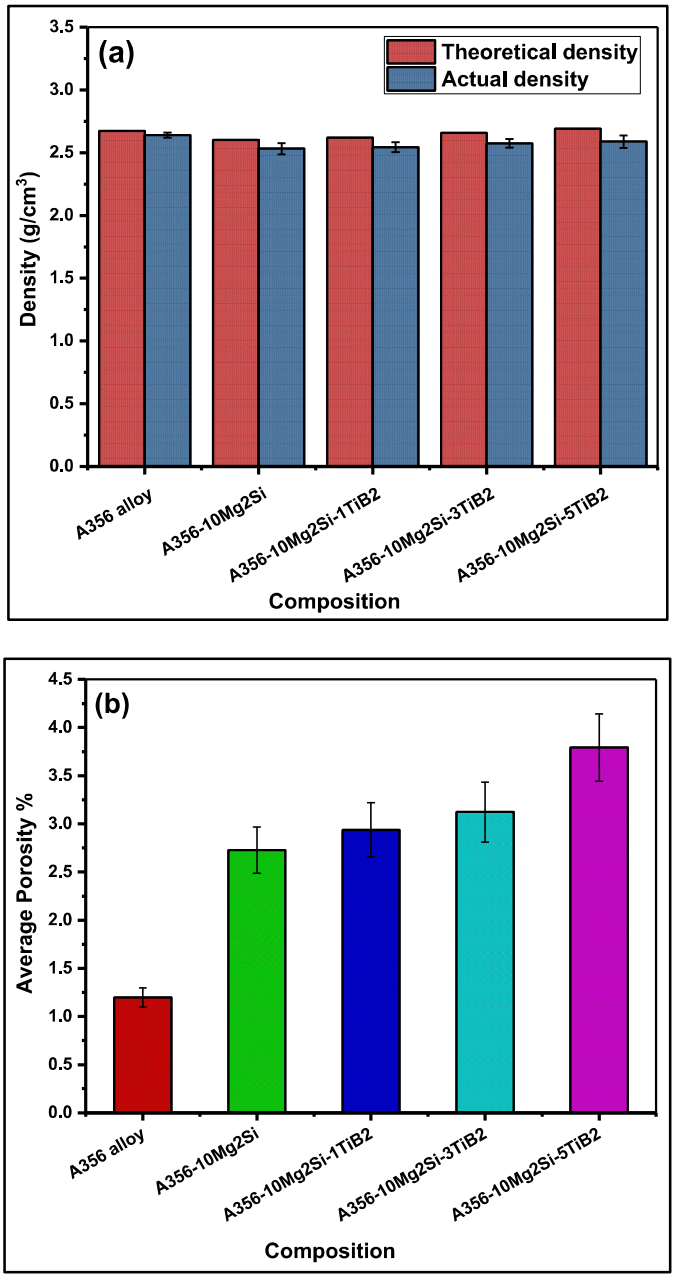

Fig. 4.2 (a) Theoretical and actual density and **(b)** average porosity percentage of A356 alloy and stir cast composites

4.4.2 Optical microscopy

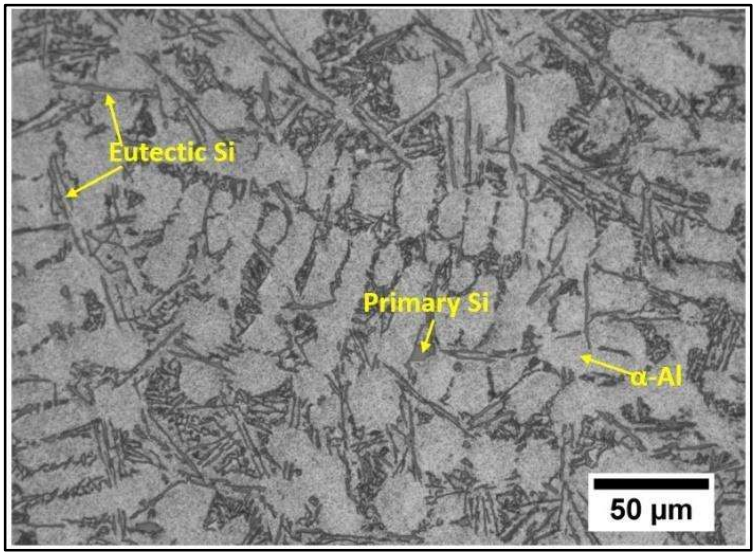

Fig. 4.3 Optical micrograph of matrix A356 alloy

Figure 4.3 presents the optical micrograph of matrix A356 alloy. It consists of α-Al, primary and eutectic Si phase. The α-Al rich phase exhibits globular and dendritic structure, whereas, the primary and eutectic Si phases exhibit irregular polygon and needle shapes, respectively.

Figure 4.4 displays the micrographs of A356-10Mg_2Si-xTiB_2 composites having different content of TiB_2 particles. The optical micrograph of A356-10Mg_2Si composite with no TiB_2 particles is shown in Fig. 4.4 (a). It reveals that primary and pseudo-eutectic Mg_2Si phases have different phase morphology. The primary Mg_2Si phase shows coarse polygon with sharp edge morphology while eutectic phases have large flake-like shape. Figs. 4.4 (b-d) show optical micrographs of hybrid composites containing 1, 3 and 5wt.% TiB_2 particles. It exhibits that A356-10Mg_2Si-TiB_2 hybrid composite with 1wt.% of TiB_2 particles, primary Mg_2Si particle are mostly unchanged and show coarse polygon morphology but the large flake-like eutectic Mg_2Si phase is significantly transformed into smaller flakes as TiB_2 particles serve as heterogeneous nuclei for Mg_2Si phase. Although insitu produced TiB_2 particles are not readily visible in optical micrographs,

this might be owing to their smaller size (submicron or nano) or the lower resolution of microscope. The hybrid composite having 3wt.% TiB_2, reveals that particle size of primary Mg_2Si phase is reduced compared with Mg_2Si particles in hybrid composite having 1% TiB_2 as revealed in Fig. 4.4 (c). Furthermore, the eutectic Mg_2Si phase is converted into a smaller flake or stick-like structure that is dispersed throughout the matrix. Fig. 4.4 (d) depicts a hybrid composite reinforced with 5 wt.% TiB_2 particles. It demonstrates that the flake-like structure of the eutectic Mg_2Si phase has been transformed into a tiny polygon or dot-like structure and is evenly distributed in the matrix. Primary Mg_2Si particles are also converted into smaller particles due to TiB_2 particles which serve as nuclei and hindered the growth of Mg_2Si particles.

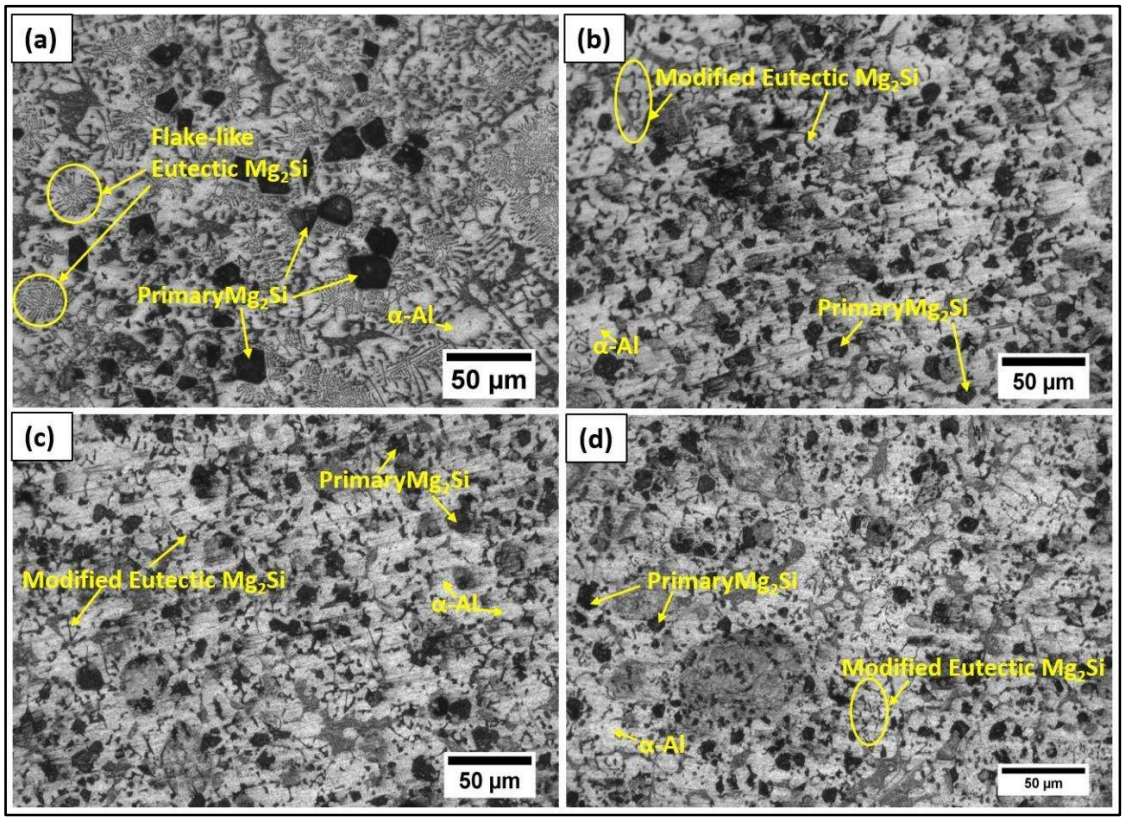

Fig. 4.4 Optical micrographs of A356-10Mg_2Si-xTiB_2 composites (a) x= 0, (b) x= 1, (c) x= 3 and (d) x= 5

4.4.3 Scanning electron microscopy

Scanning electron microscopy (SEM) of hybrid composites is also carried out to further investigate the microstructural features with varying amount of TiB_2 phase as presented in Fig. 4.5. These micrographs show the same microstructural features as observed in the optical microstructures except the TiB_2 phase, which was not very clear in Fig. 4.4. Whereas, TiB_2 particles are clearly observed when studied under SEM even hybrid composite with 1 wt.% TiB_2 in A356-10Mg_2Si-TiB_2 due to high resolution of SEM. However, with high amount of TiB_2 (3 and 5wt.%), increase in particles is clearly observed in the SEM micrographs. But with increase in TiB_2, clustering of these particles is observed, which is seen at places in A356-10Mg_2Si-3TiB_2 and A356-10Mg_2Si-5TiB_2 hybrid composites. It signifies that TiB_2 particles are segregated at the interface, significantly modifying the phase morphology and size of Mg_2Si particles. [123].

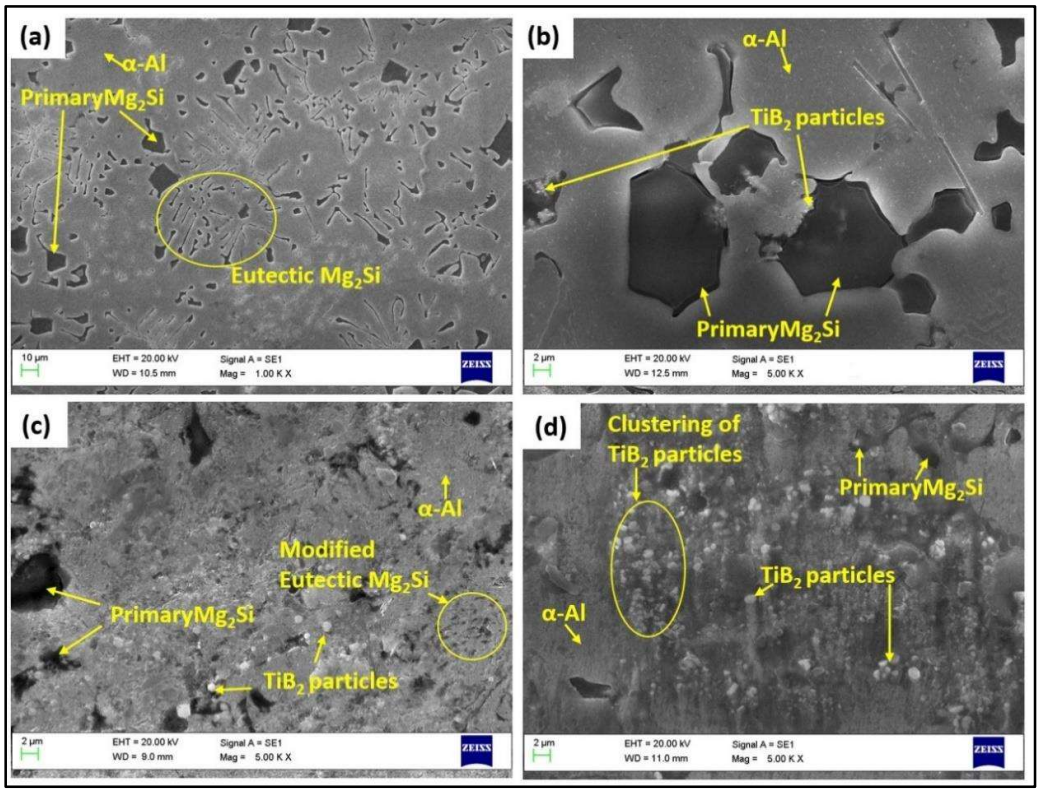

Fig. 4.5 SEM micrographs of A356-10Mg_2Si-xTiB_2 composites with varying content of TiB_2 particles (a) x= 0, (b) x= 1, (c) x= 3 and (d) x= 5

Further, it is also noticed that some TiB_2 particles are embedded in the Mg_2Si phase, which demonstrate that these particles act as nuclei for matrix and Mg_2Si particle. These nuclei improve the solidification of the Mg_2Si particle and its distribution in matrix phase [49]. The even dispersion of the Mg_2Si particles can substantially improve the mechanical and wear behaviour of hybrid composites.

The SEM microstructures of stir cast A356-10Mg_2Si-3TiB_2 are presented in Fig. 4.6 (a, b). TiB_2 particles are shown to be agglomerated around the primary Al and Mg_2Si phases, with some TiB_2 particles embedded in the Mg_2Si particles. Because of the low solid percentage in the melt, the TiB_2 particles were rejected during solidification by developing solids of the Al matrix and Mg_2Si phase [49]. Some of the TiB_2 particles are consequently incorporated into the Mg_2Si particles as it also serves as nuclei for the Mg_2Si phase. Figure 4.6 (c, d) depicts the EDS analysis of the hybrid A356-10Mg_2Si-3TiB_2 composite, confirming that the Mg_2Si and TiB_2 phases were successfully formed.

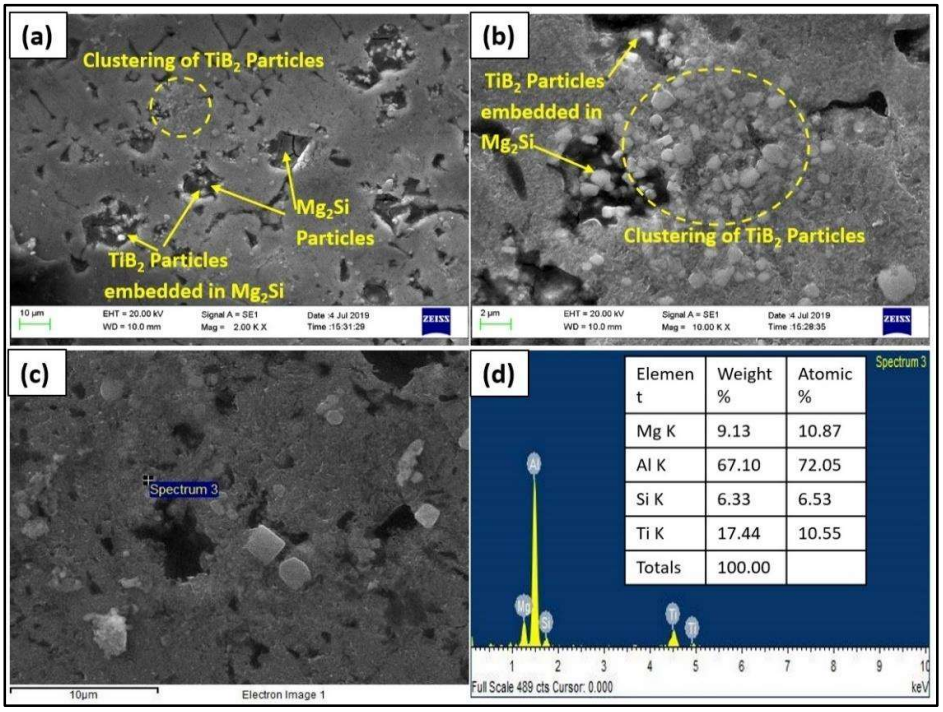

Fig. 4.6 SEM micrographs of A356-10Mg_2Si-3TiB_2 hybrid composites at (a) low magnification (b) high magnification (c) point of EDS in SEM image of A356-10Mg_2Si-3TiB_2 and (d) corresponding EDS spectrum

4.4.4 Elemental analysis and particle size & their distribution

Fig. 4.7 displays the elemental mapping derived from the EDS analysis of each of the elements in the hybrid composite. The elements in the hybrid composite, namely Si, Mg, Ti, and B, are distributed uniformly throughout.

Figure 4.8 represents the particle size of Mg_2Si in the hybrid composites with varying amount of TiB_2 content. The particle size has been measured from the SEM micrographs. Primary Mg_2Si particle size decreased to 8.3 µm from 16 µm with increase in TiB_2 content from 0 to 5wt.% (Fig. 4.8 (a)). While, eutectic Mg_2Si phase is reduced from 12.3 µm to 5.5 µm with increase of TiB_2 content (Fig. 4.8 (b)). However, the TiB_2 particles size histogram is presented in Fig. 4.9, indicating that most of the particles are within a range of 0.2-1.4 µm with a mean size of 0.6 µm in hybrid composites.

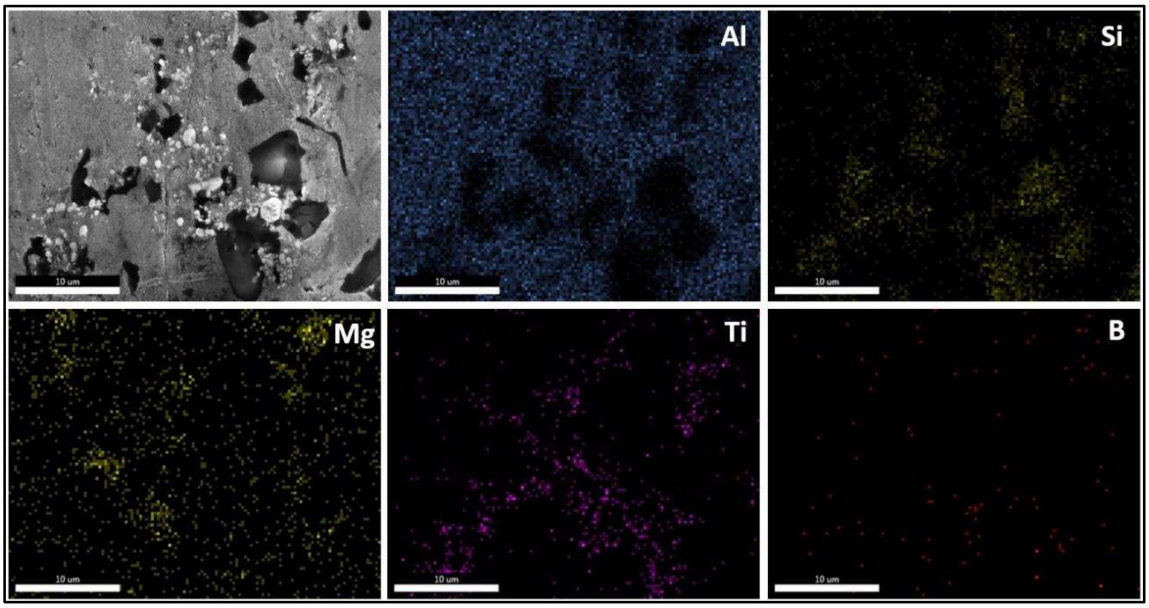

Fig. 4.7 SEM micrograph of A356-10Mg_2Si-3TiB_2 hybrid composites and corresponding mapping of elements Al, Si, Mg, Ti and B

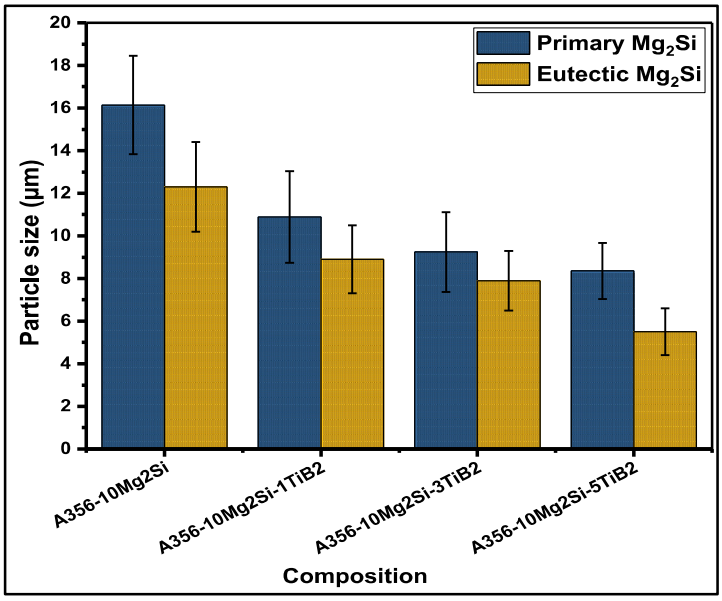

Fig. 4.8 Average particle size of primary Mg_2Si and eutectic Mg_2Si phase in different composites

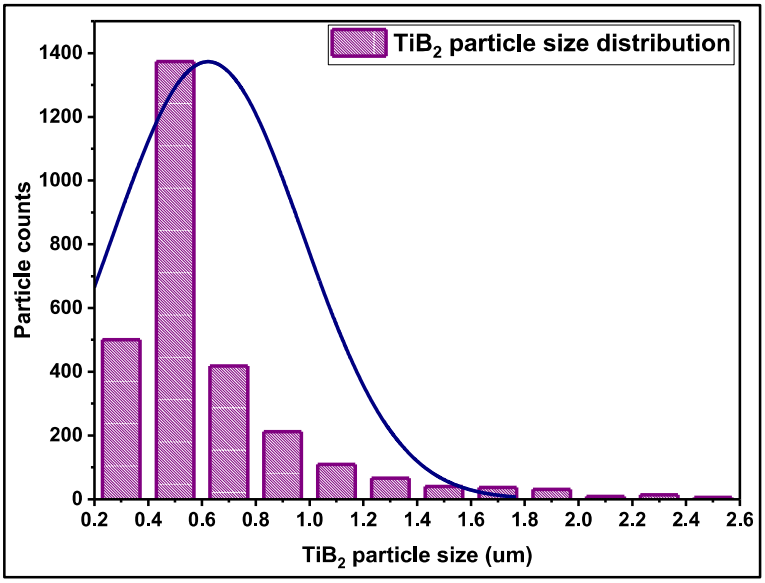

Fig. 4.9 The TiB_2 particles size distribution histogram in hybrid composite.

4.4.5 Hardness Properties

Figure 4.10 presents the Vickers hardness value of base A356 alloy and composites with varying TiB_2 content (0 to 5wt.%). The hardness value of composites is improved when the second phase reinforcement TiB_2 is incorporated in the A356-Mg_2Si composite. It continuously increases with increase of TiB_2 phase in hybrid composites. Hardness value of hybrid composite having 5wt.% TiB_2 in A356-10Mg_2Si composite is

increased to 110.48 HV as compared to 60.36 HV and 81.26 HV of matrix A356 alloy and A356-10Mg_2Si composite respectively. The hardness value is improved owing to uniform distribution and refinement of Mg_2Si and matrix phase. The higher hardness of reinforcements than the A356 alloy is also significantly contributed to the improvement in hardness of composites.

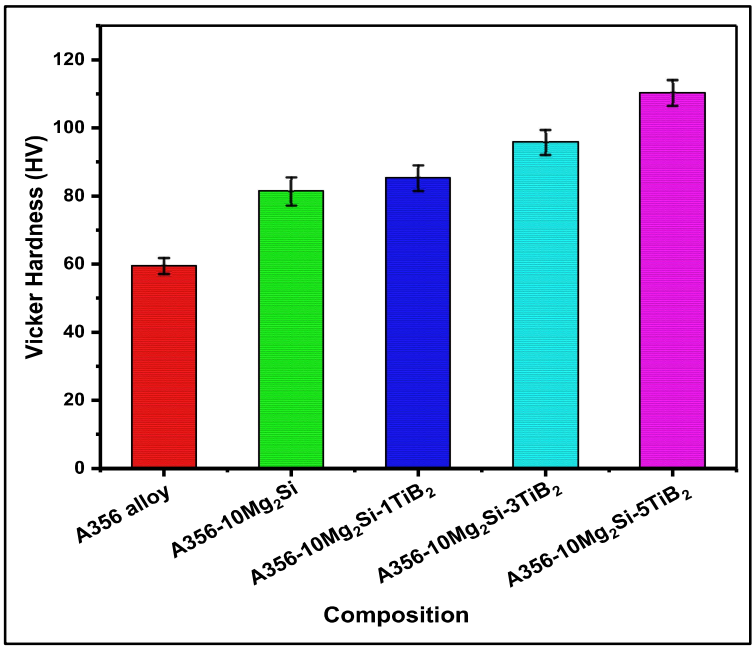

Fig. 4.10 Hardness of A356 alloy and composites

4.4.6 Tensile properties

Figure 4.11 displays stress-strain curves of A356 alloy and stir cast composites having various weight percentages of TiB_2 particles. These curves have been used to evaluate ultimate tensile strength (UTS) and percentage elongation of different compositions. Fig. 4.12 displays the graph plotted using the data of UTS and % elongation from the tensile curve. The A356-10Mg_2Si composite shows drastically reduced ductility when Mg is added to A356 alloy. This is due to a higher percentage of intermetallic compound Mg_2Si in matrix which favours microcracks initiation and propagation through matrix and eutectic phase for failures of the composite. From the

figures it is evident that all the mechanical characteristics i.e., UTS and percentage elongation of hybrid composites improve with increase of the TiB_2 content. Enhancement in percentage elongation of A356-10Mg_2Si-5TiB_2 hybrid may be due to grain refinement by TiB_2 particles. The greater resistance to fracture propagation caused by grain refinement may also be responsible for the improvement in ductility. Similar results were also noticed in the ZrB_2 reinforced Al composite case by N. Kumar et al. and Tian et al.[83, 124].

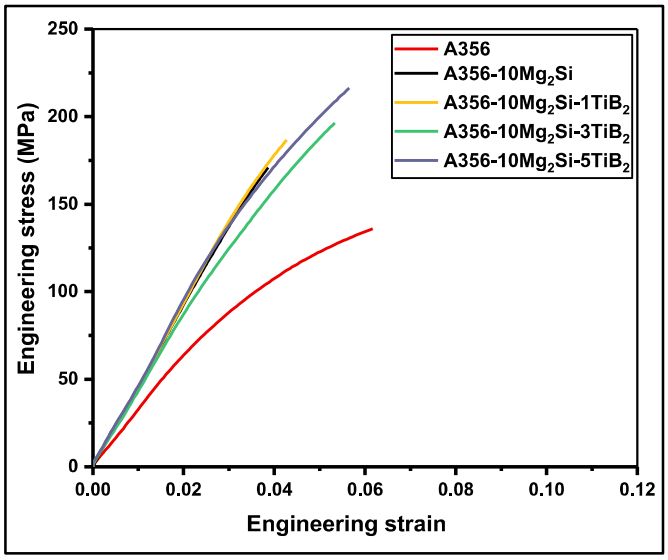

Fig. 4.11 Engineering stress-strain curve A356 alloy, A356-10Mg_2Si, and A356-10Mg_2Si-xTiB_2 composites

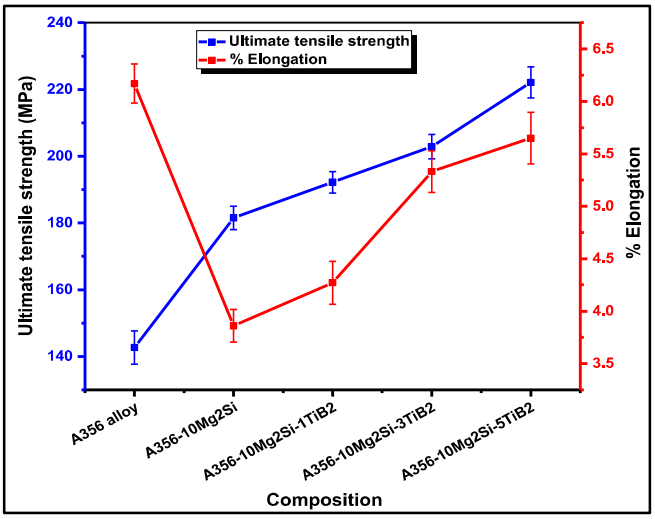

Fig. 4.12 Tensile strength and percentage elongation of A356 alloy, A356-10Mg_2Si, and A356-10Mg_2Si-xTiB_2 composites

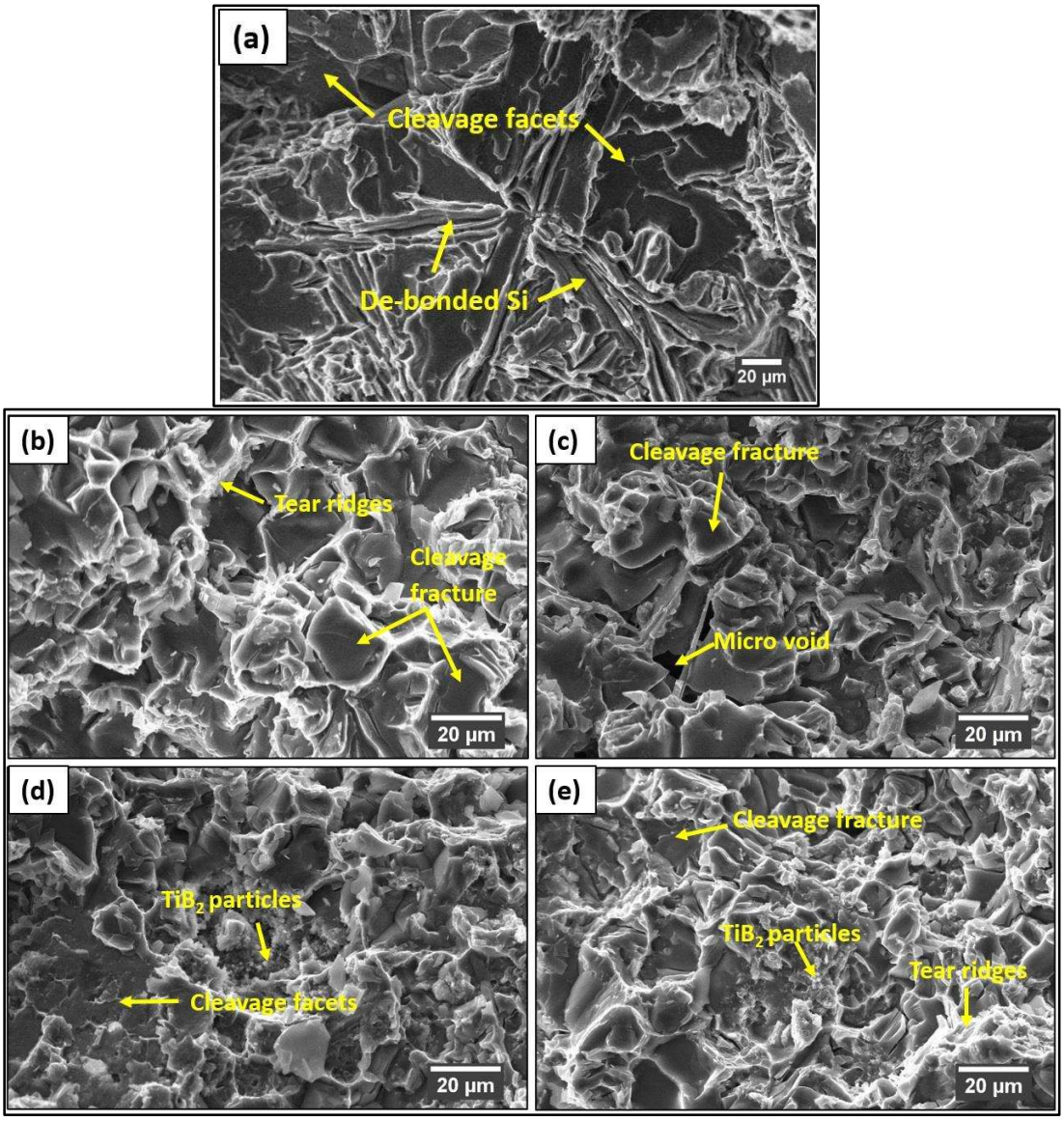

Fig. 4.13 Fracture surface of base alloy (a) A356 (b) A356-10Mg_2Si composite and hybrid composite A356-10Mg_2Si-xTiB_2 with varying TiB_2 content (c) x= 1 (d) x= 3 (e) x= 5

SEM fractography of the A356 alloy tensile sample is shown in Figure 4.13 (a). Cracks start at the locations of defects such as shrinkage porosity and widen as the load increases. Facets in eutectic Si are seen in the fractured surface. Figure 4.13 (b) displays SEM micrograph of fractography of A356-10Mg_2Si. We can see that the fractography of composite has brittle fracture due to the crack initiated at the site of coarse Mg_2Si particles that, leads to debonding, and hence, elongation is drastically decreased compared with the matrix alloy. It might also be related to fracture of eutectic Mg_2Si

having flake like shapes, resulting in brittle fracture of the composite. Stress concentration at the sharp corners of Mg_2Si particles generate microcracks, which lead to the premature failure of the composites. Figure 4.13 (c-e) depicts the fracture surface of stir cast hybrid composites. It can be shown that the addition of TiB_2 phase alters and refines the primary and eutectic Mg_2Si, resulting in reduced crack initiation and propagation rates and consequently, improved mechanical characteristics [39].

4.5 MICROSTRUCTURAL AND MECHANICAL CHARACTERISTICS OF HYBRID COMPOSITES IN COOLING SLOPE CAST CONDITIONS

4.5.1 Density and porosity measurement

Figure 4.14 (a) and (b) presents the theoretical density, actual density and porosity percentage of cooling slope (CS) cast matrix alloy and composites with varying amounts of TiB_2 particles respectively. Fig. 4.14 (a) indicates that with addition of Mg, density of the composite reduces owing to the low density of Mg_2Si phase (1.99 g/cm^3). However, porosity in the composite increases compared with the alloy as presented in Fig 4.14 (b). It can be attributed to the large freezing range of the composites. Higher density of secondary reinforcement TiB_2 phase, (4.52 g/cm^3) increases the density of hybrid composite. Porosity in the hybrid composite slightly decreases with increasing TiB_2 particles up to 3wt.% owing to even distribution of TiB_2 phase in the matrix. However, hybrid composite containing 5wt.% TiB_2 particles have maximum porosity, which is around 3% which could be due to agglomeration of TiB_2 particles and difference in coefficient of thermal expansion. [39]. Further, it has been described that the applying CS casting technique reduces the shrinkage porosity and micro voids because of lower temperature of melt slurry in the mold[123]. Thus, CS casting technique can improve the mechanical behaviour of composites by reducing the casting defects.

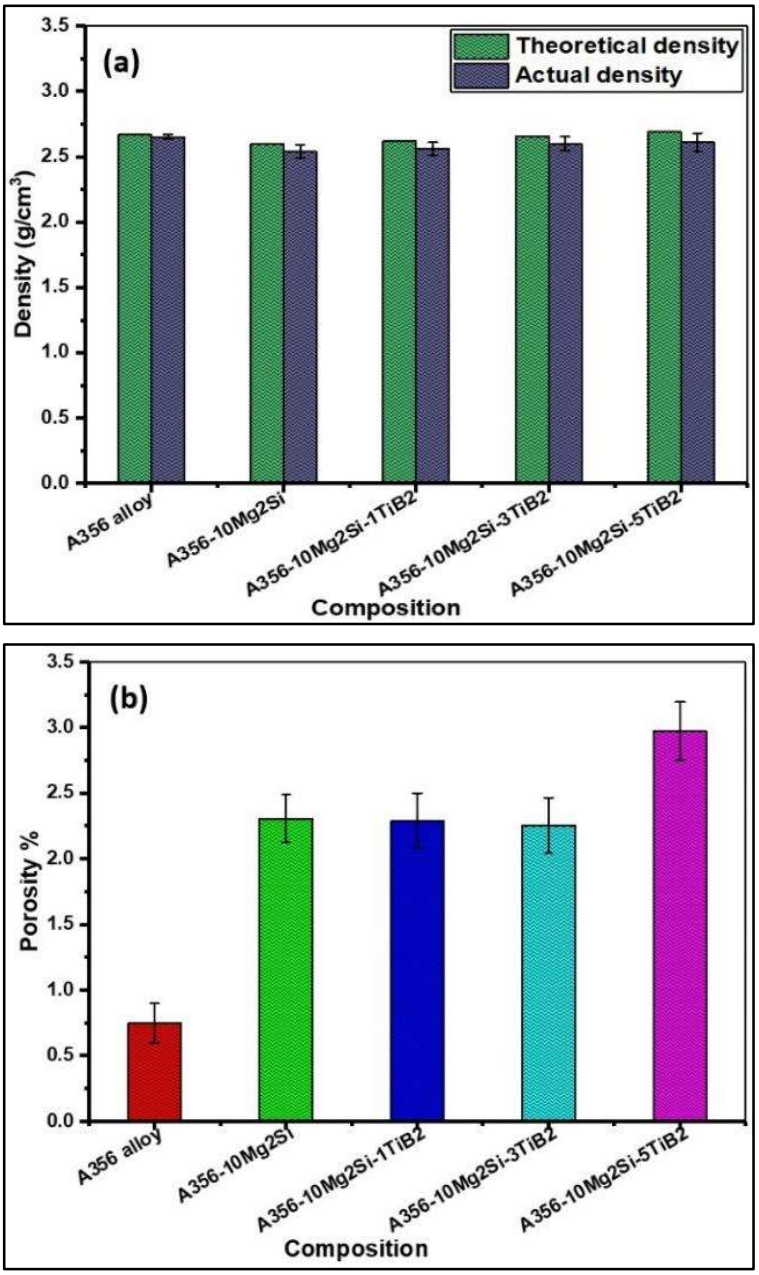

Fig. 4.14 (a) Theoretical and actual density and **(b)** average porosity percentage of CS cast A356 alloy and composites

4.5.2 Optical microscopy

Figure 4.15 shows the micrographs of composites with varying amounts of TiB_2 particles. The optical micrograph of A356-Mg_2Si composite without TiB_2 particles is shown in Fig. 4.15 (a). It is evident that primary and pseudo-eutectic Mg_2Si phase have different phase morphology. The primary Mg_2Si phase showing coarse polygon while

eutectic phase has flake-like morphology. Some of eutectic phase modified by into smaller stick and dot like morphology by CS casting but primary phase showing course polygon morphology.

The optical image of CS cast A356-10Mg_2Si-1TiB_2 composite is shown in Figure 4.15 (b). The coarse and sharp-edged primary Mg_2Si particles transformed into finer and almost spherical shapes, while the coarse flake structure of the eutectic Mg_2Si phase transformed into little scattered stick like structure. Transformation in the shape and size of primary as well as eutectic Mg_2Si phase could be owing to the presence of TiB_2 particle as it provides nucleation site for Mg_2Si phase. These sites in the melt hinders the development of Mg_2Si phase and enhance the dispersion of the phase. Another reason behind the refinement is that the Mg_2Si phase pushed at the interface during solidification and hinders the growth of Mg_2Si phase.

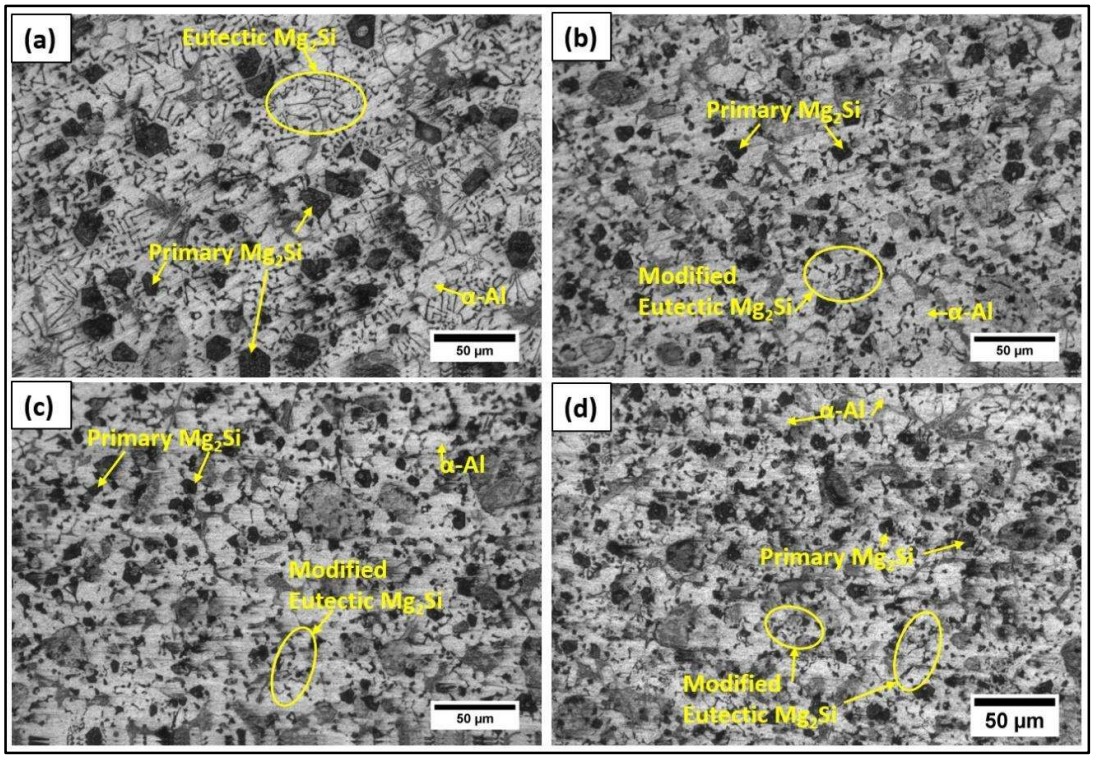

Fig. 4.15 Optical micrographs of hybrid composites A356-10Mg_2Si-xTiB_2 with varying content of TiB_2 particles (a) x= 0 (b) x= 1 (c) x= 3 (d) x= 5

Figure 4.15 (c) and (d) present the optical micrograph of CS cast hybrid composites containing 3 wt.% and 5 wt.% TiB_2 particles respectively. With increased TiB2 content in A356-10Mg2Si composite, the particle size of primary and eutectic Mg_2Si phase decreases. TiB_2 particles are not visible in optical micrographs since they are nano and submicron in size. Refinement of the Mg_2Si phase could be owing to fragmentation of the Mg_2Si phase through shearing of molten slurry during melt move on the cooling slope plate under gravitational force [10]. As the temperature difference is very high between the cooling plate and molten metal, rapidly solidify the melt and increases the solid percentage in melt. The large solid and TiB_2 content in the melt acts as a nucleation site, which enhances the nucleation of insitu Mg_2Si, resulting in finer Mg_2Si phase distributed uniformly in the composite [47].

4.5.3 Scanning electron microscopy

The SEM micrography of A356-10Mg_2Si-xTiB_2 hybrid composite with varying TiB_2 content was also carried out to understand microstructural features in a better way and are displayed in Fig. 4.16. Fig. 4.16 (a) presents the A356-10Mg_2Si composite consisting of polygon shaped primary Mg_2Si phase and flake and stick like structure of eutectic phase. Fig.4.16 (b) shows the hybrid composite having 1% TiB_2 particles. TiB_2 particles are clearly visible at few places due to low amounts of particles. Fig. 4.16 (c) and (d) show the hybrid composite containing 3% and 5% TiB_2 particles respectively. TiB_2 particles are evenly dispersed in the composite containing 3wt.% TiB_2, however, considerable particle agglomeration has been observed in few regions in the composite containing 5% TiB_2 particles. Segregation propensity of the TiB_2 particles increases with the increasing particle content because these are pushed at the grain boundaries during solidification. Moreover, morphology and size of primary and eutectic Mg_2Si phases

were refined by adding the TiB_2 phase in A356-10Mg_2Si composite. This is associated with the inoculant behaviour of TiB_2 particles, which were embedded in the Mg_2Si phase in a few spots, indicating that it acts as the nucleus for Mg_2Si phase [125]. These nucleation site improve the solidification of Mg_2Si particles restricting the growth which leads to the refinement and even dispersion of particles in the composite. Besides the effect of TiB_2 phase on Mg_2Si phase, CS casting technique also affects the refinement, phase morphology and distribution of Mg_2Si phase. With the increase of TiB_2 phase, grain size and morphology transformation increase, indicating that TiB_2 phase has a certain influence on refinement of eutectic Mg_2Si phase. Thus, employing CS casting technique along with the TiB_2 phase remarkably refines and transform the phase morphology of Mg_2Si phase due to the fragmentation of the phases under the shear action of cooling plate while melt flowing over the plate under gravity.

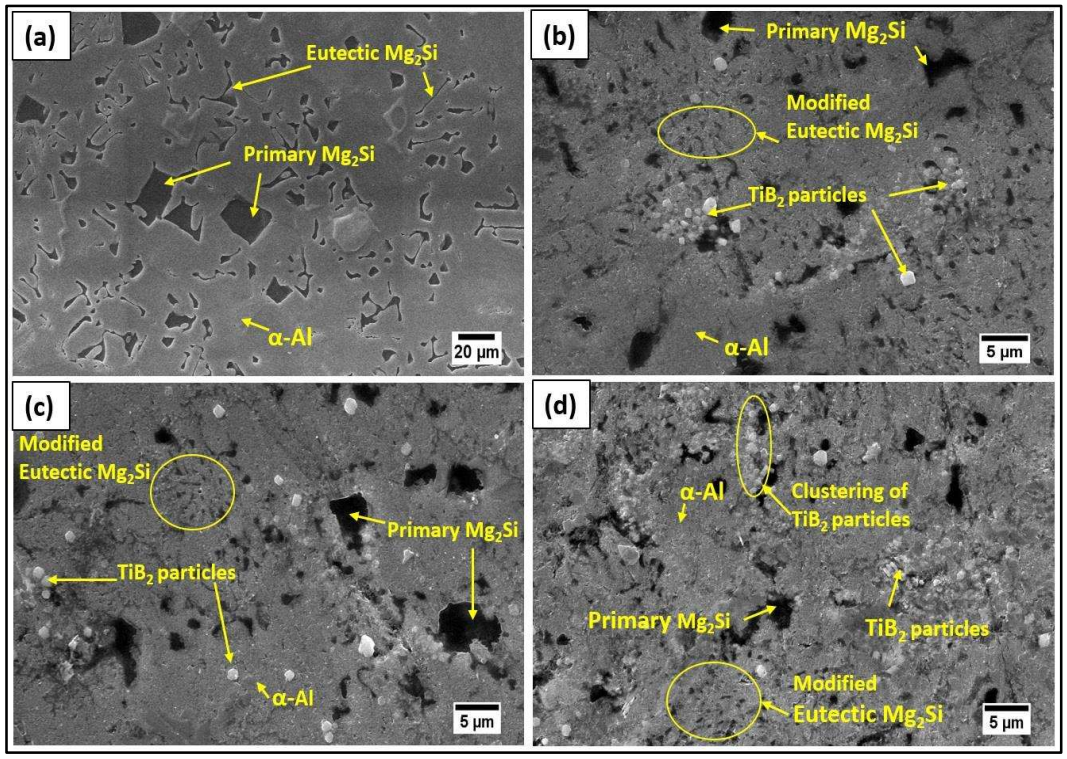

Fig. 4.16 SEM micrographs of hybrid composites A356-10Mg_2Si-xTiB_2 with varying content of TiB_2 particles (a) x= 0 (b) x= 1 (c) x= 3 (d) x= 5

Primary Mg_2Si phase refines into smaller polygon shape and almost all the flake like eutectic phase converted into dot like phase, precipitated uniformly throughout the composite. Segregation of the TiB_2 phase can also be reduced by CS casting because of the high solute content in melt slurry at exit of slope plate. Because of high solute content in molten metal, it quickly solidifies in mould decreases the rejection of TiB_2 particle during solidification. This indicates that CS casting technique can significantly refine and transform the shape of Mg_2Si phase and improve the distribution of the phases. Figure 4.17 (a) and (c) displays the SEM micrographs of A356-Mg_2Si-xTiB_2 hybrid composite and Fig. 4.17 (b) and (d) displays the EDS spectrum of corresponding points in the micrograph of the hybrid composite A356-10Mg_2Si-1TiB_2 respectively. The EDS spectrum also confirms the formation of insitu Mg_2Si and TiB_2 phase.

4.5.4 Particle size analysis

Particle size of α-Al, primary Mg_2Si, eutectic Mg_2Si phase and TiB_2 particle size distribution in single reinforced composite and hybrid composites with varying amount of TiB_2 phase are shown in Fig. 4.18. Particle size of α-Al reduced from 21.5 µm to 10.5 µm and primary Mg_2Si particle size decreased from 12.2 µm to 6.6 µm with increase in TiB_2 content from 0 to 5wt.% (Fig. 4.18 (a)). While, eutectic Mg_2Si phase is decreased from 11.2 µm to 4.9 µm with increase of TiB_2 content. The TiB_2 particle size has been measured form the SEM micrographs. The TiB_2 particles size distribution in the hybrid composite is presented in Fig. 4.18 (b) which indicates that the size of TiB_2 particle is mostly in the range of 0.2-1.0 µm with mean size of 0.41 µm in hybrid composites.

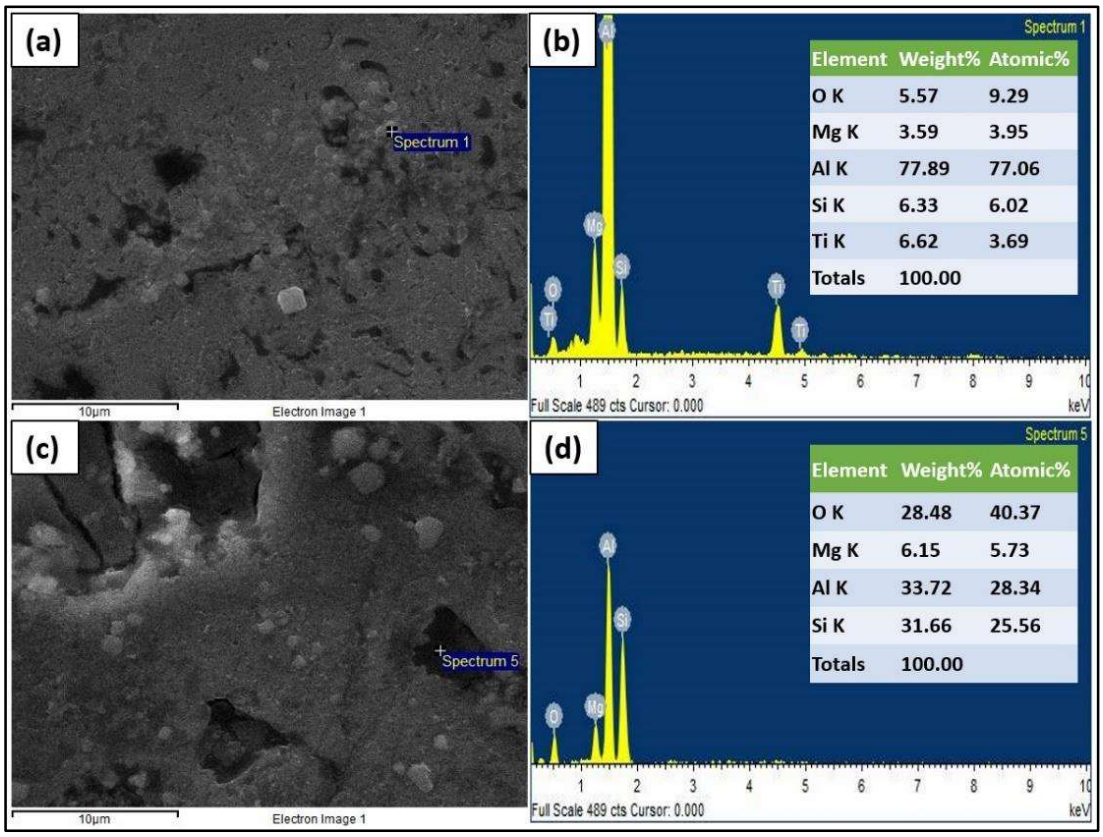

Fig. 4.17 SEM micrographs of hybrid composites A356-10Mg_2Si-xTiB_2 (a) and (c), EDS spectrum of the corresponding points in micrograph (b) and (d) respectively

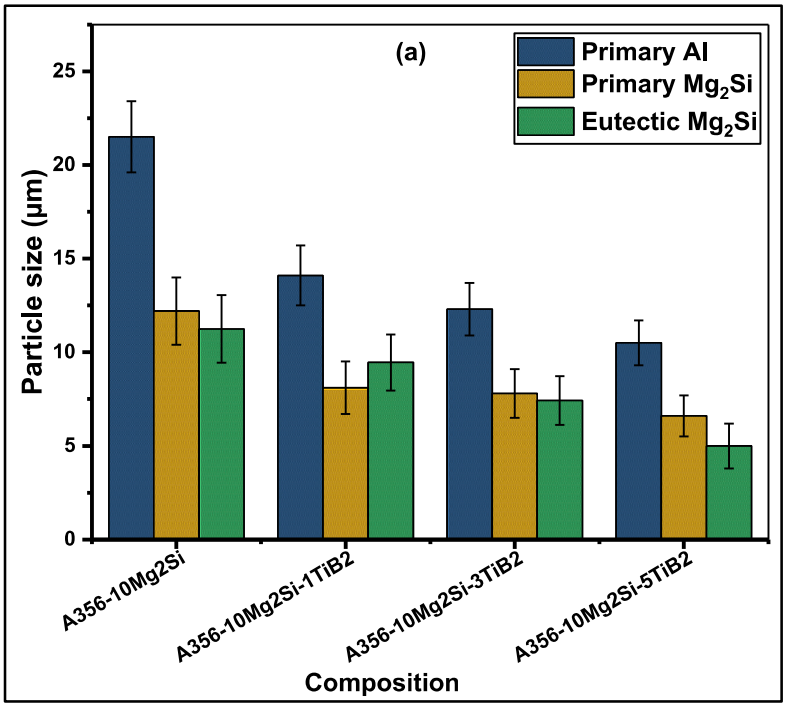

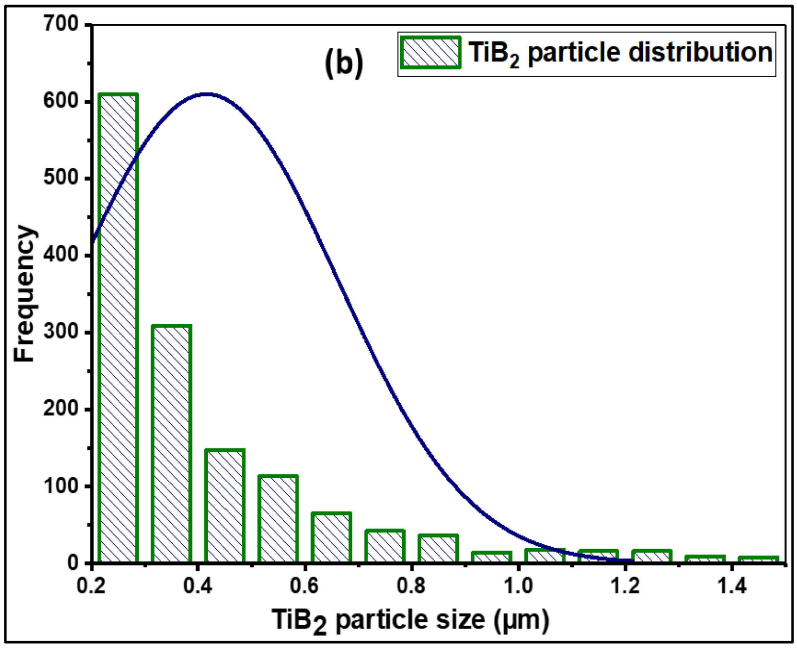

Fig. 4.18 (a) Average particle size of α-Al, primary Mg_2Si and eutectic Mg_2Si composites in A356-10Mg_2Si-xTiB_2 with varying content of TiB_2 particles **(b)** TiB_2 particle size distribution in A356-10Mg_2Si-5TiB_2

4.5.5 Hardness

Figure 4.19 presents the Vickers bulk hardness of matrix alloy A356 and A356-10Mg_2Si composite and A356-10Mg_2Si-xTiB_2 hybrid composite contain varying amount of TiB_2 particles. Average hardness of matrix A356 alloy is 62.6 HV while A356-10Mg_2Si composite has hardness of 89.4 HV. Hardness value of hybrid composite continuously increases with the addition of secondary reinforcement phase. With increased TiB_2 content from 1% to 5%, the hardness of hybrid composite improved from 94.8 HV to 116.2 HV. The enhancement in hardness of the hybrid composite can be owing to two reasons. Firstly, increase of the wt.% of reinforcement and refinement of matrix and Mg_2Si phase by TiB_2 particles in the hybrid composite. Second is the application of CS casting technique which also help in the refinement of eutectic phase and increases the distribution of the reinforcement particle as it reduces shrinkage porosity and segregation of reinforcement particles at grain boundary. Thus, combined

effect of CS casting technique and addition of TiB_2 phase in A356-Mg_2Si composite remarkably increases the hardness of hybrid composite.

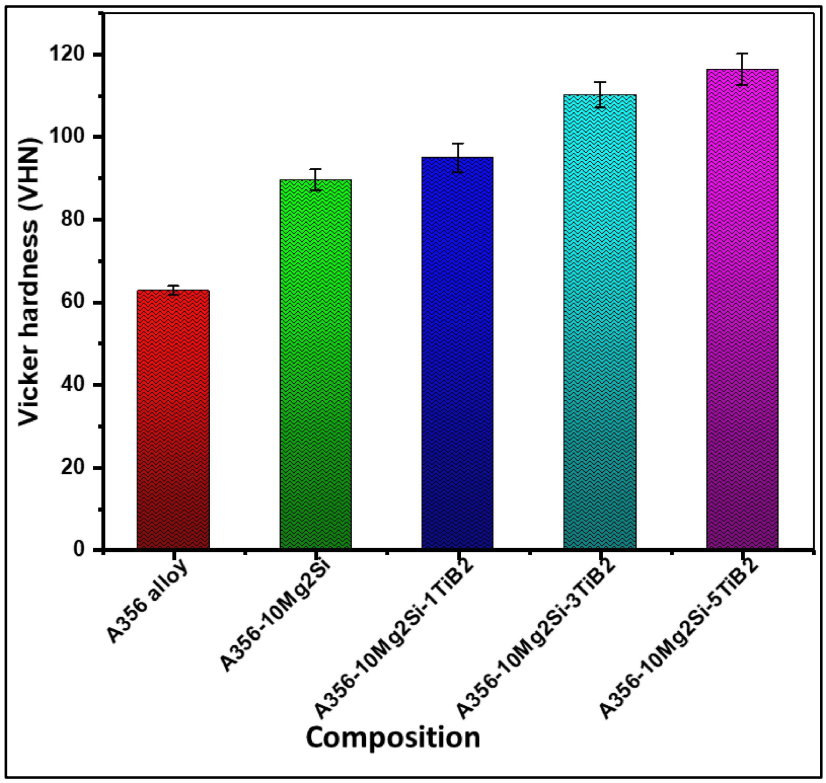

Fig. 4.19 Vickers hardness of A356 alloy and A356-10Mg_2Si-xTiB_2 composites

4.5.6 Tensile properties

Tensile curve of matrix alloy A356, composite A356-10Mg_2Si and hybrid composite A356-10Mg_2Si-xTiB_2 with various weight percentage of TiB_2 phase are displayed in Fig. 4.20 (a). A356-10Mg_2Si composite without TiB_2 content exhibits poor percentage elongation and less improvement in ultimate tensile strength. With increase of TiB_2 content in hybrid composite, tensile strength and percentage elongation increases gradually as presented in Fig. 4.20 (b). Maximum tensile strength and percentage elongation were noticed in hybrid composite contains 5 wt.% TiB_2 particles. Ultimate tensile strength of A356-10Mg_2Si-5TiB_2 hybrid composite increases by 59% and 28% as compared to the A356 alloy and A356-10Mg_2Si composite respectively. Elongation percentage of A356-10Mg_2Si-5TiB_2 hybrid composite increased by 55% compared with

the A356-10Mg_2Si composite. This can be attributed to the finer Mg_2Si phase and TiB_2 particles almost distributed evenly in matrix.

The matrix and Mg_2Si phases were refined by the addition of TiB_2 particles as it acts as nucleation site. Refinement of the matrix and Mg_2Si phase improve the tensile properties by increasing the ductility of hybrid composites. Application of CS casting technique also helps the refinement of eutectic phase as it converted from flake like morphology into short sticks and dot like morphology and uniform distribution of finer particle ultimately increases the mechanical behaviour of composites. Thus, tensile strength and ductility of hybrid composite increases by applying CS casting method and adding TiB_2 particles due to the following reasons: first, strengthening due to grain refinement and refinement of Mg_2Si phase increases the grain boundary regions which restrict the movement of dislocations during deformation and leads to the better strength and elongation of hybrid composites. According to hall-Petch relation, finer the grain size more the strength of material. In addition, uniform distribution of Mg_2Si and TiB_2 particles using CS casting method reduces the tendency of crack generation and propagation and decreases the failure of materials. Since the particle size of TiB_2 phase is much smaller than 1μm distributed evenly in the composite, it hinders the movement of dislocation and form dislocation loop to strengthen the composite as per the Orowan strengthening mechanism. Eutectic Mg_2Si phase refined into dot like structure by CS casting process. Most of the dot eutectic Mg_2Si phase having size less than 1μm also contribute in the strengthening of composite by impeding the movement of dislocation. In addition, Mg_2Si and TiB_2 phases have lower thermal coefficient than the matrix which induces the residual strain at the matrix-reinforcement interface. These residual strains generate dislocations surrounding the particles, increases the dislocation density and also helps in the strengthening of hybrid composite[105, 109]. Therefore, tensile strength and

ductility of A356-10Mg_2Si-5TiB_2 hybrid composite synthesized by CS casting method significantly increased.

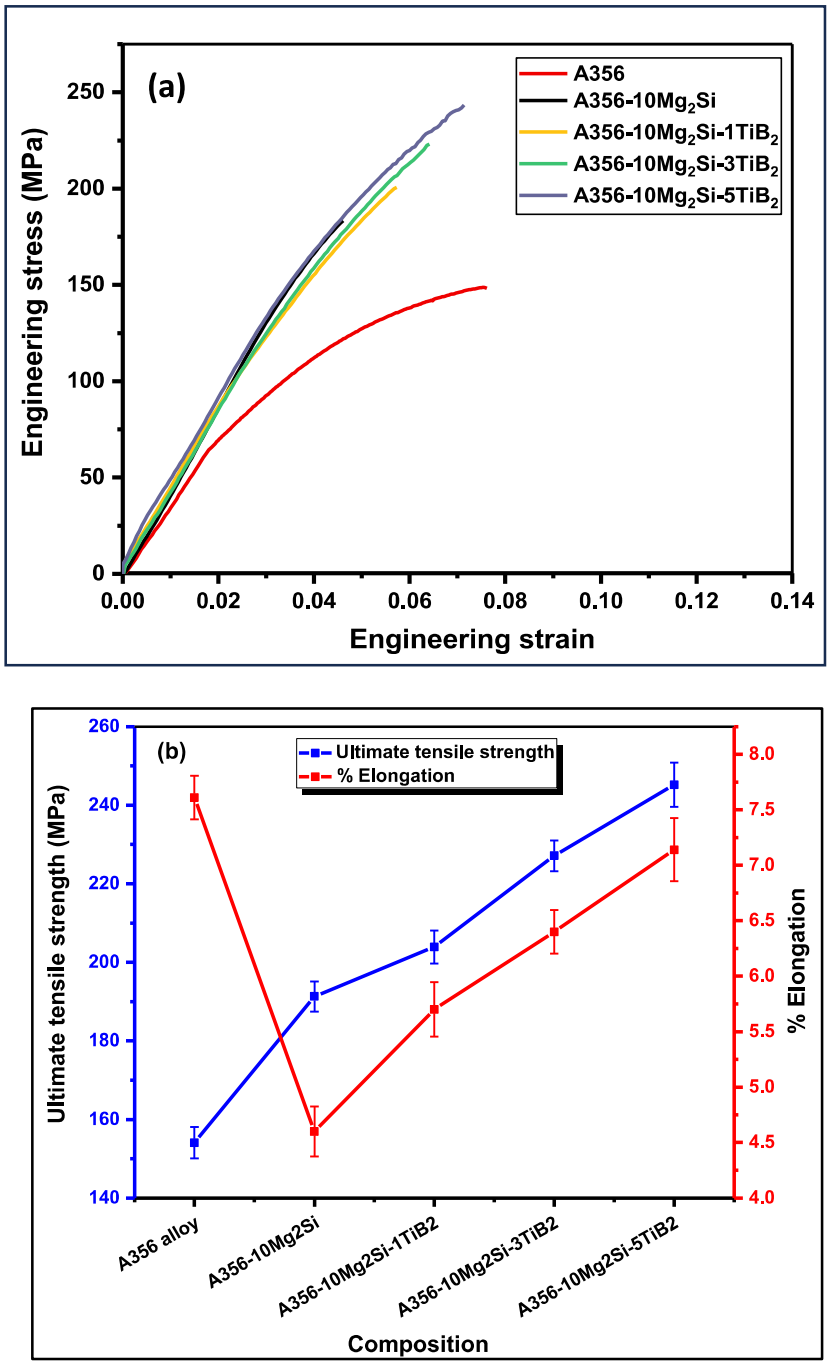

Fig. 4.20 (a) Engineering stress-strain curve and **(b)** Tensile strength and percentage elongation of A356 alloy, A356-10Mg_2Si, and A356-10Mg_2Si-xTiB_2 composites

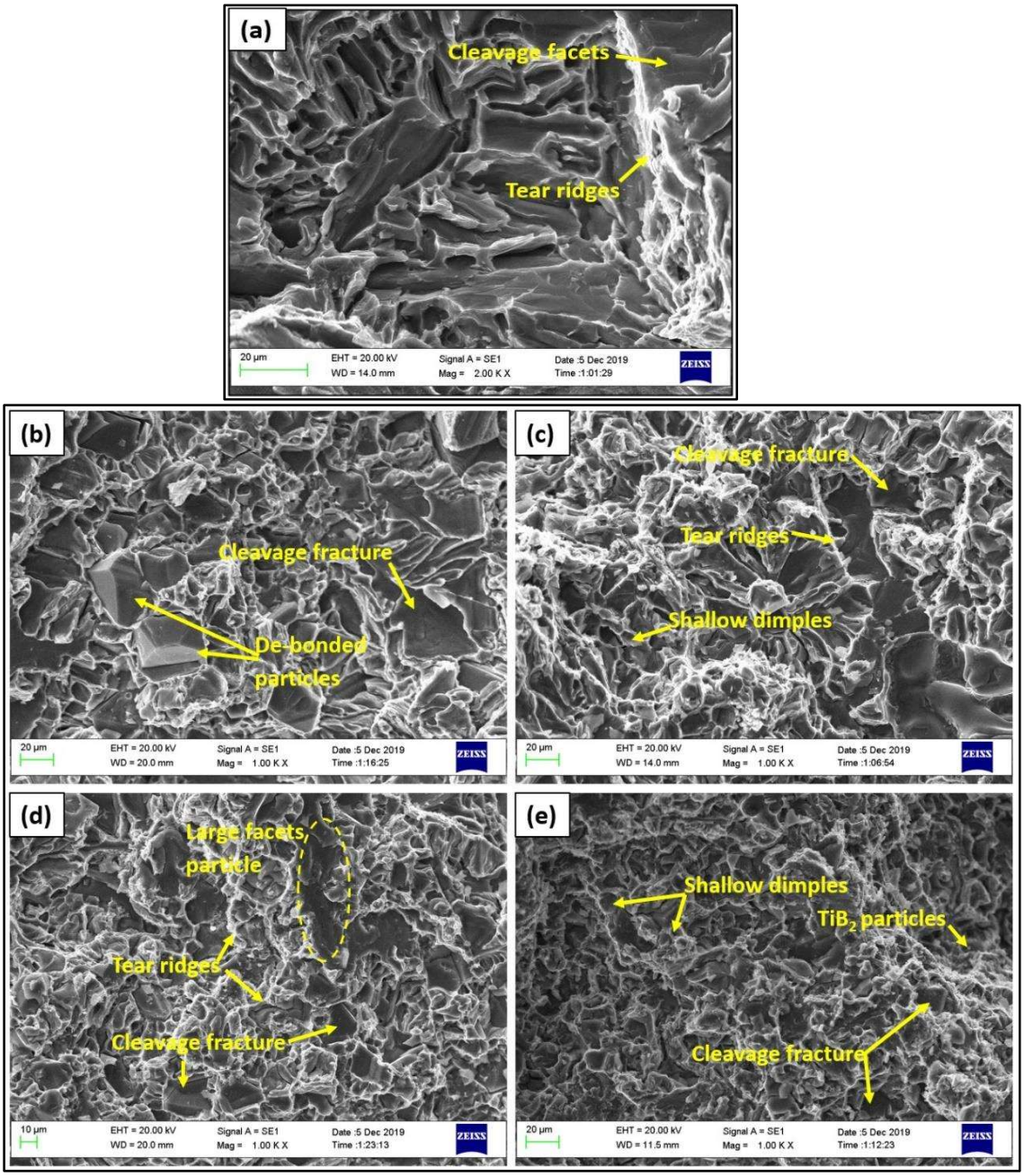

Fig. 4.21 Fractography of (a) matrix A356 (b) A356-10Mg_2Si composite and hybrid composite A356-10Mg_2Si-xTiB_2 with varying TiB_2 content (c) x= 1 (d) x= 3 (e) x= 5

Figure 4.21 presents the SEM fractography of A356 alloy A356-10Mg_2Si, and A356-10Mg_2Si-xTiB_2 hybrid composites. Fig. 4.21 (a) shows the fractography of A356 alloy and it can be noticed that the cracks are initiated at eutectic Si phase and propagated through Si phase that leads to fracture and debonding of Si phase. Some cleavage facets observed along with the dimples in Al phase indicate mixed mode of fracture of matrix

alloy. Fig. 4.21 (b) shows the fractography of A356-10Mg_2Si composite and it indicates that cracks are initiated at the brittle primary Mg_2Si and large eutectic Mg_2Si phase, showing brittle fracture. The fracture surface showing decohered and cracked particles which reveals that coarse Mg_2Si phase has cleavage fracture due to its brittle nature and pre-cracked structure.

The fractography of hybrid composites A356-10Mg_2Si-xTiB_2 with varying TiB_2 content are shown in Figs. 4.21 (c-e). The fractured surface of hybrid composite still showing brittle fracture but cleavage planes are smaller owing to matrix and Mg_2Si phase refinement by the addition of TiB_2 phase and application of CS casting. With increasing TiB_2 particle addition, fine dimples are observed whereas decohered particles are reduced considerably due to fine particles, which results in increases percent elongation. By adding 5% TiB_2 particles, uniform dispersion of TiB_2 particle and clustering of particles at few places are found along with the tear ridges and cleavage facets as revealed in Fig. 4.21 (e). Therefore, elongation of hybrid composite increases from 4.6% to 7.1% with increase of TiB_2 content from 0 to 5%. The quasi-cleavage fracture of the hybrid composite is characterised by brittle fracture of Mg_2Si phase and shallow dimples (ductile fracture) of the Al matrix. Therefore, adding TiB_2 in composite and employing CS casting method changes fracture characteristics of hybrid composite from brittle fracture to mixed mode of fracture i.e., partly ductile, and partly brittle fracture.

4.6 COMPARATIVE STUDY OF MICROSTRUCTURAL FEATURES AND MECHANICAL PROPERTIES OF STIR CAST AND CS CAST COMPOSITES

4.6.1 Microstructural features

Figure 4.22 (a) and (b) show the particle size of primary and eutectic Mg_2Si phase respectively in stir as well as CS cast composites. It is evident that primary as well as

eutectic Mg_2Si phase is refined in all the composites. The refinement of primary and eutectic Mg_2Si phase in A356-10Mg_2Si-5TiB_2 increased by around 25% and 10 % respectively by application of CS casting route. The rapid cooling of melt on cooling plate and fragmentation of dendrites by shearing generate large heterogeneous nucleation sites. The nuclei grow but fast solidification restrict the growth of matrix as well as Mg_2Si phase.

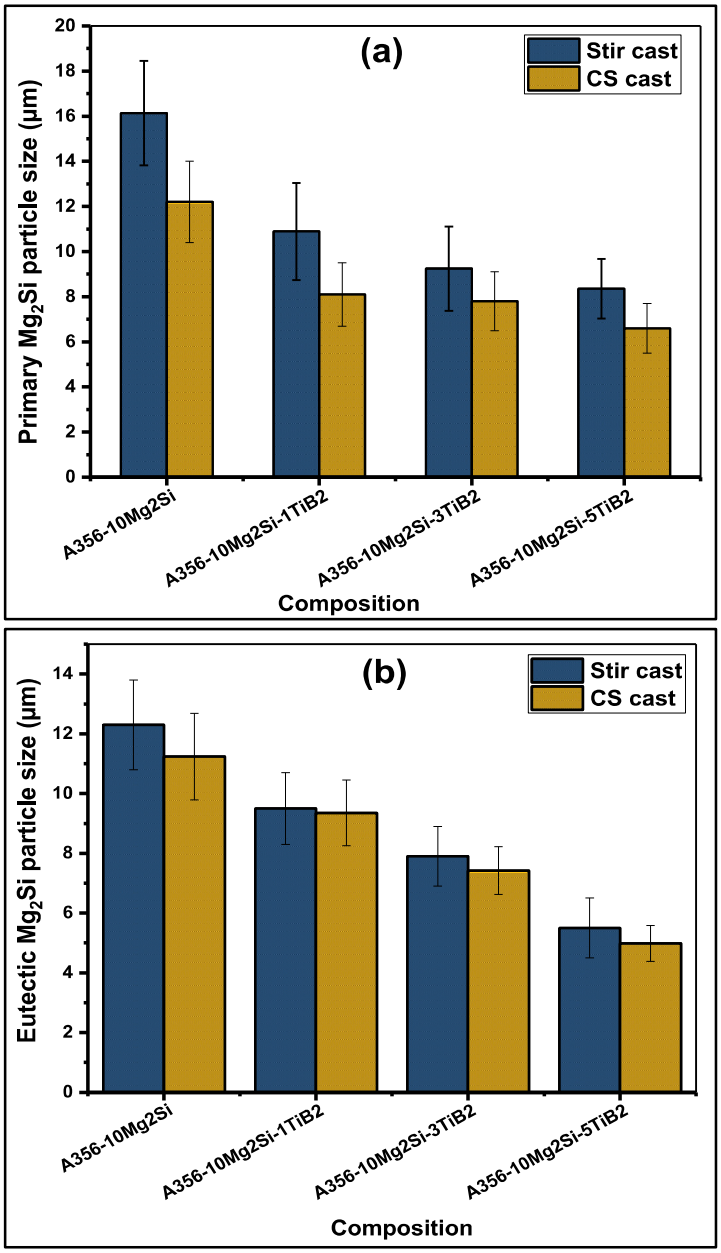

Fig. 4.22 (a) Average particle size of primary Mg_2Si and **(b)** eutectic Mg_2Si phase in stir cast and CS cast composites

Fig. 4.23 shows the TiB_2 particle size distribution in A356-10Mg_2Si-5TiB_2 hybrid composite synthesized through the stir casting and CS casting. Figure indicates that particle size distribution in CS cast composite is better than the stir casting. The average particle size is approximately 0.45 µm in CS cast hybrid composite compared with the 0.67 µm in stir cast hybrid composites.

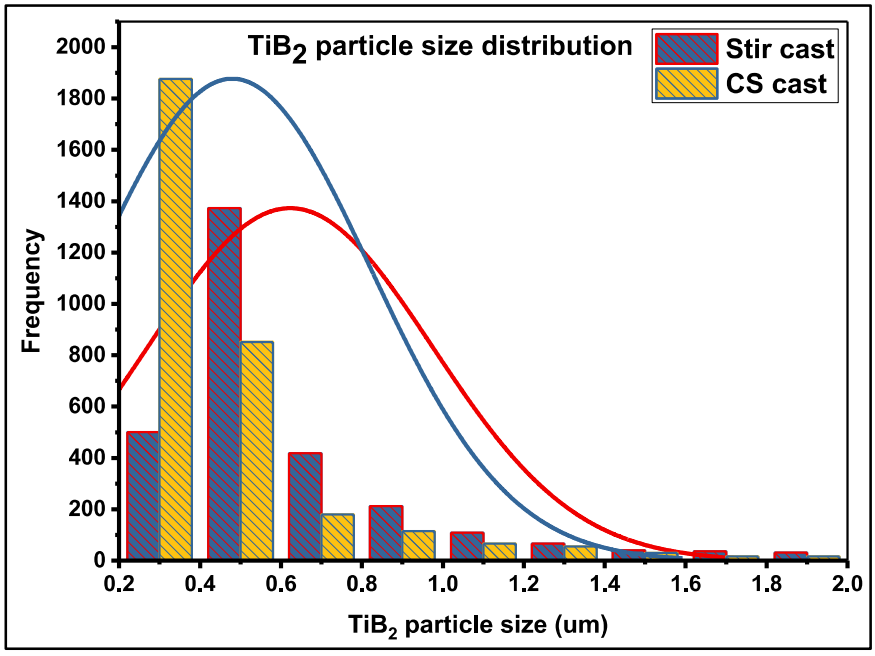

Fig. 4.23 The TiB_2 particles size distribution in A356-10Mg_2Si-5TiB_2 hybrid composite

4.6.2 Mechanical properties

Figure 4.24 depicts the hardness of stir and CS cast composites, and it is clear that CS cast composites have higher hardness than stir cast composites. This is due to improved refinement and dispersion of reinforcing particles. Finer reinforcement phase dispersed uniformly into the matrix are responsible for higher hardness. Figures 4.25 (a) and (b) show the ultimate tensile strength and percentage elongation of samples cast through stir and CS casting technique. When compared to stir cast composites, CS cast composites have better tensile strength and percentage elongation. Improvement in the tensile strength is about 11% and percent elongation is about 25% in CS cast A356-

$10Mg_2Si$-$5TiB_2$. Therefore, the refinement of Mg_2Si phase leads to enhancement in tensile strength and percent elongation. Besides this lower porosity in CS cast composites also improves the strength and ductility as porosity plays significant role in crack initiation.

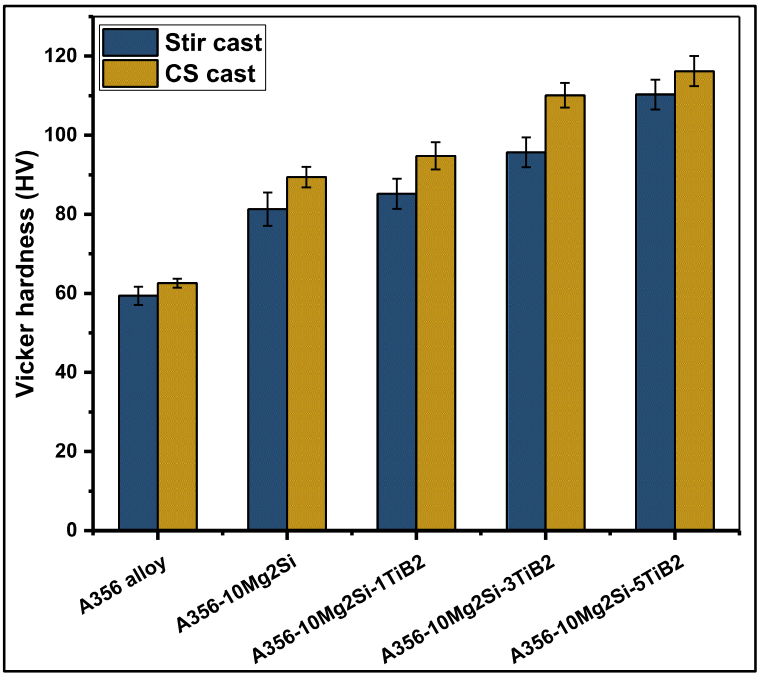

Fig. 4.24 Vickers hardness of A356 alloy and A356-$10Mg_2Si$-$xTiB_2$ composites

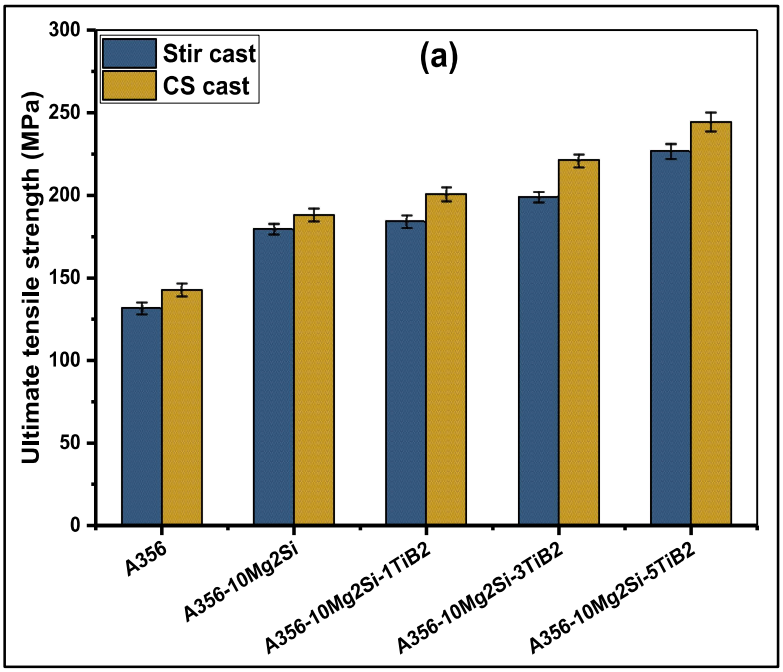

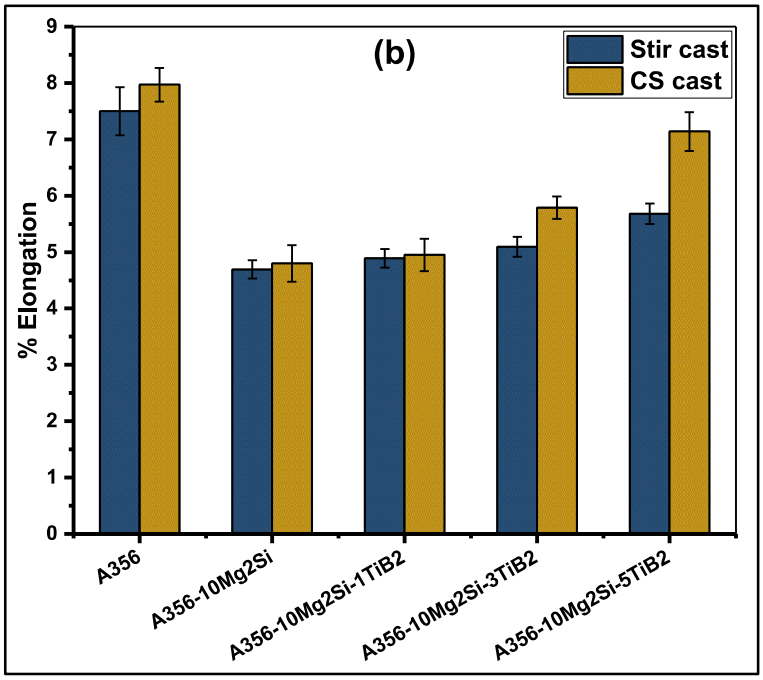

Fig. 4.25 (a) Tensile strength and **(b)** percentage elongation of A356 alloy, A356-10Mg_2Si, and A356-10Mg_2Si-xTiB_2 hybrid composites

4.7 Summary

The effect of different TiB_2 compositions on microstructural and mechanical characteristics of insitu A356/Mg_2Si-TiB_2 hybrid composites in stir cast and CS cast conditions have been studied.

The following conclusions can be derived from the results analysis:

- Insitu formed TiB_2 particles in A356-Mg_2Si-TiB_2 hybrid composite refine the matrix and Mg_2Si phase. The shape of primary Mg_2Si transformed from coarse polygon to smaller polygon and large flakes of eutectic Mg_2Si phase transformed into finer flats and dot like polygons as TiB_2 particles act as nucleation site for matrix as well as Mg_2Si phase.
- Application of CS casting technique also helps in the refinement as the grain size further reduced and phase morphology of α-Al and Mg_2Si phase transformed significantly. The CS casting method enhances the nucleation and favours the

fragmentation of dendrites leading to the development of non-dendritic structure due to shearing action.

- The CS cast composites have lower porosity compared with the stir cast composites due to lower shrinkage porosity and micro voids also help in the enhancement of properties of CS cast hybrid composites
- Grain size of α-Al reduced from 21.5 μm to 10.5 μm, primary Mg_2Si from coarse polygon (~12 μm) to smaller and spherical polygon (~ 6.6 μm) and eutectic Mg_2Si from large flake (~ 11.7 μm) to smaller flake (~ 5 μm) and dot like morphology.
- Hardness of hybrid composite increased 85% and 30% compared with the A356 alloy and A356-10Mg2Si composite respectively in CS cast condition.
- Tensile strength and percentage elongation of CS cast hybrid composite improved by 28% and 55% respectively in comparison with A356-10Mg_2Si composite.
- The fracture surface reveals that in both the casting routes hybrid composite has quasi-cleavage fracture, characterized by brittle of Mg_2Si phase and shallow dimples of Al phase.